Rating of seismicity and reconstruction of the fault geometries in northern Tien Shan within the project "Seismic Hazard Assessment for Almaty"

J. Torizin, G. Jentzsch, P. Malischewsky, J. Kley, N. Abakanov, A. Kurskeev

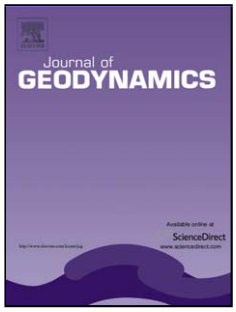

Title: Rating of seismicity and reconstruction of the fault geometries in northern Tien Shan within the project "Seismic Hazard Assessment for Almaty"

Authors: J. Torizin, G. Jentzsch, P. Malischewsky, J. Kley, N. Abakanov, A. Kurskeev

PII: S0264-3707(09)00097-0
DOI: doi:10.1016/j.jog.2009.09.030
Reference: GEOD 924

To appear in: *Journal of Geodynamics*

Please cite this article as: Torizin, J., Jentzsch, G., Malischewsky, P., Kley, J., Abakanov, N., Kurskeev, A., Rating of seismicity and reconstruction of the fault geometries in northern Tien Shan within the project "Seismic Hazard Assessment for Almaty", *Journal of Geodynamics* (2008), doi:10.1016/j.jog.2009.09.030

Rating of seismicity and reconstruction of the fault geometries in northern Tien Shan within the project "Seismic Hazard Assessment for Almaty"

J. Torizin[1], G. Jentzsch[1], P. Malischewsky[1], J. Kley[1], N. Abakanov[2], A. Kurskeev[2]

[1]Institute of Geosciences, Friedrich-Schiller University Jena

[2]Institute of Seismology, Almaty

Abstract

The project "Seismic Hazard Assessment for Almaty" has a main objective to improve existing seismic hazard maps for the region of northern Tien Shan and especially for the surroundings of Almaty and to generate a new geodynamic model of the region.

In the first step a composite seismic catalogue for the northern Tien Shan region was created, which contains about 20,000 events and is representative for strong earthquakes for the period back to the year 500. For the period of instrumental observation 1911-2006 the catalogue contains data for earthquakes with a body wave magnitude larger than 4. For smaller events with magnitudes up to 2.2 the data are only available since 1980. The composite catalogue was created on the basis of several catalogues from the United States Geologic Survey (USGS), local catalogues from the Kazakh National Data Centre (KNDC) and the USSR earthquake catalogue. Due to the different magnitudes used in several catalogues a magnitude conversion was necessary.

Event density maps were created to rate the seismicity in the region and to identify seismic sources. Subsurface fault geometries were constructed using tectonic model which uses fault parallel material flow and is constrained by GPS data. The fault geometry should improve the estimation of the expected seismic sources from seismic density maps.

First analysis of the earthquake catalogue and the density maps has shown that nearly all large events are related to fault systems. Annual seismicity distribution maps suggest different processes as the cause for the seismic events. Apart from tectonics, also fluids play a major part in triggering of the earthquakes.

Beneath the Issyk-Kul basin the absence of strong seismic activity suggest aseismic sliding at the flat ramp in a ductile crust part and low deformation within the stable Issyk-Kul micro continent which underthrust the northern ranges of Tien Shan. First results suggest a new partition of the region in tectonic units, whose bounding faults are responsible for most of the seismic activity.

1. Introduction

During the last 150 years Almaty was destroyed several times by strong earthquakes. The last earthquake with a magnitude > 8.0 occurred in 1911. The city is located on a large active fault zone of the northern Tien Shan. This fault called Almaty-Fault is covered by mezozoic and cainozoic sediments and does not crop out at the surface but its activity is shown by the high seismicity in the region. Located on the northern range of Zailijsky Alatau (the northernmost ridge of Tien Shan) Almaty is also endangered by debris flows which can be triggered by weaker earthquakes. With regard to the population of more than one million people the quantification of the seismic hazard has to be improved. The work present here is a part of the international project "Seismic Hazard Assessment for Almaty". The objective of the project is to improve the existing hazard maps and to create an up-to-date geodynamic model of the region. For our research we use data from different origins. There are geological data like geologic maps and tectonic maps (DELVAUX et al. 2001), geophysical data like a Bouguer anomaly map from surveys in the USSR in the late ´70 (, data from the GRACE satellite mission like EGM 2008 (PAVLIS et al. 2008), GPS data (UNAVCO 2008), local seismic catalogues and seismic models from receiver functions (VINNIK et al. 2004, 2006) and seismic tomography (MAKAROV et al. 2005). In this work parts of the seismic hazard assessment are presented.

2. Investigation area, geodynamic and geological setting

The area of interest is located in Central Asia in northern Tien Shan and encompasses the two northernmost ridges of the mountain Zailijsky Alatau and Kungej Alatau and parts of sediments basins - the Ili basin and the Issyk-Kul basin. The north to south extension of the research area is nearly 150 km and east to west 200 km. Almaty is situated in the centre of the research area (Fig. 1).

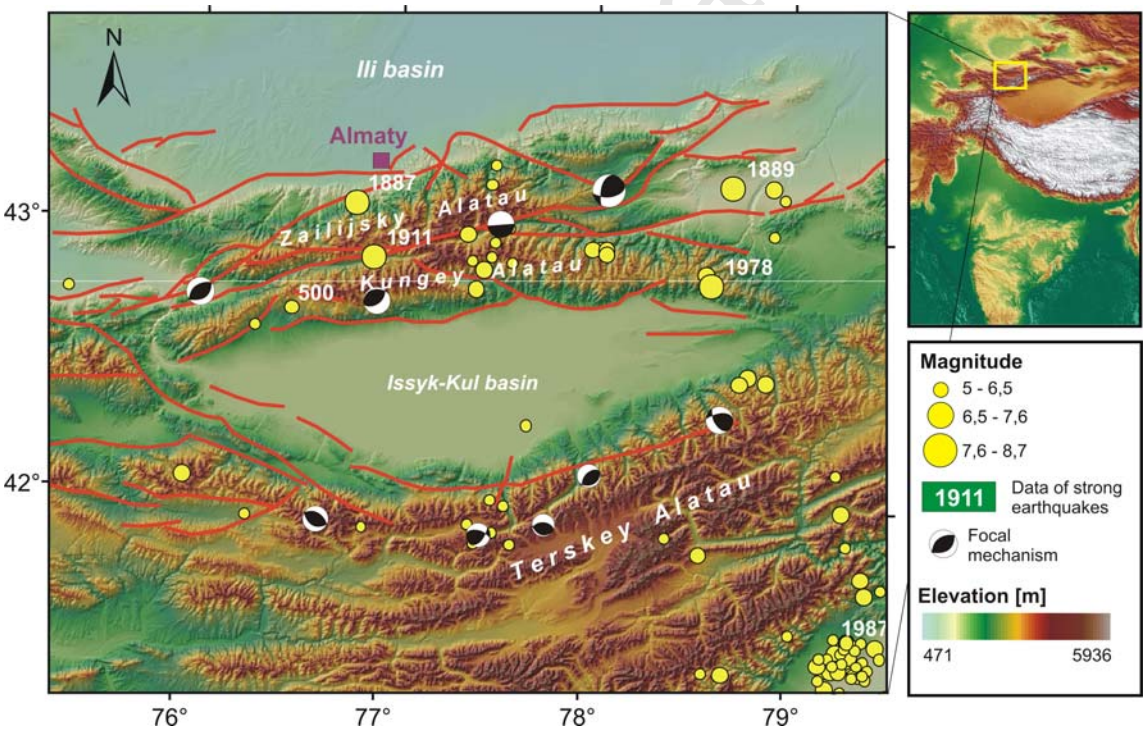

Fig. 1. General overview of the investigated area. Red lines are active faults after DELVAUX et al. 2001. Yellow circles are significant earthquakes in the region. Some focal mechanisms are given for strong earthquakes.

The present day structure of northern Tien Shan consists of roughly E-W oriented ranges separated by parallel sediment basins. Ranges and basins are separated by big thrust faults. Northern Tien Shan ranges consist of metamorphic rocks but also of intrusive and volcanic formations. Sediments that fill the basins are conglomerates, sandstones, silts and clays (MAKAROV et al. 2005). Sediment thickness reaches up to 4.5 km in the southern part of the Ili-Basin and is approximately 4 km in Issyk-Kul basin (KOSTENKO 2001).
The geodynamic situation in this region is controlled by the ongoing collision of India and Eurasia. After a building of the Tien Shan "pre-orogenic surface" in Cretaceous, tectonic activity started in Oligocene (AVOUAC et al. 1993). Apatite Fission Track method shows an activity peak in northern Tien Shan within the past 3 Myr. (BUSLOV et al. 2008). The current geodynamic situation is given by the underthrusting of the Tien Shan from

south-east by the stable Tarim block, whereas Pamir is working as an indenter from the south and south-west. Compression tectonics led to a reactivation of ancient normal faults (BUSLOV et al. 2004). The average shortening of Tien Shan is supposed to be approximately 200 km (MOLNAR 1993; ABDRAKHMATOV et al. 1996; MAKAROV et al. 2005). Recent GPS measurements show that alarge part of recent collision deformation will be accumulated here several thousand kilometres away from the collision suture (REIGBER 2001). GPS measurements show horizontal displacements of up to 20 mm/yr in the southern part of Tien Shan and 1-3 mm/yr in northern Tien Shan (ABDRAKHMATOV et al. 2001). The observed deformations are actually discussed as a result of the rotational behaviour of the stable Issyk-Kul micro-continent and the development of strike slip faults (BUSLOV et al. 2004).
Stress accumulation is followed by high seismicity consequently. The earthquake focal mechanisms from Harvard CMT Earthquake Catalogue show thrust faults with strike slip components which also point to the regional compression regime with escape tectonics. The regional stress map is exclusively based on focal mechanism solutions. The predominant strike direction of the compression axis is approximately N-S, almost perpendicular to the east-west strike direction of the mountain range (MAKAROV et al. 2005). Scientific research in the past relates the strong earthquakes to the big fault systems in North and South Tien Shan (GHOSE & HAMBURGER 1998; MOLNAR et al. 1987, 2000; ABDRAKHMATOV et al. 1996; MAKAROV et al. 2005) due to the fraction processes around the faults. Smaller earthquakes cannot be allocated to certain tectonic structures and seem to occur everywhere at shallow depths. Events with magnitudes smaller then 3.0 are defined as "background" seismicity. Big scaled seismic hazard assessment for Northern Eurasia was already done by ULOMOV (1999).

3. Seismic hazard assessment

Seismic hazard requires the knowledge of possible epicentre locations, occurrence and strength. The process of seismic hazard assessment consists usually of four steps. The first step is the characterization of the seismic sources. The second step is the estimation of earthquake recurrence from seismic catalogues. The third step is the estimation of ground motion attenuation from macro seismic data (e. g. intensity maps from bigger earthquakes). The last step is finally the calculation of probability of the exceedance for events of certain magnitudes for a certain time period. All these steps can be done when a seismic catalogue and necessary geologic information are available (CORNELL 1968; REITER 1990; CHEN & SCAWTHORN 2002).

4. Seismic catalogues

Regarding the central issues of the hazard assessment, in the first step the composite seismic catalogue for the northern Tien Shan region was created, which goes back to the time until 500 A. D. for strong earthquakes. For the period of instrumental observation 1900-2006 the catalogue contains data for earthquakes with a magnitude bigger than 4. For smaller events with magnitudes up to 2.2 the data are only available since 1980 after the establishment of a suitable seismic network in the region. For the compilation of this catalogue local catalogues from the Kazakh National Data Centre (KNDC), NEIC-catalogue from the U.S. Geological Survey (USGS) and published regional catalogues from the former USSR (KONDORSKAYA et al. 1977) were used. The instrumental data for the last two years can be updated continuously from the KNDC online catalogue. In several catalogues different magnitudes were used to characterize the earthquake strength. After the composition of these catalogues three magnitude classes were available. The body wave magnitude m_b, which was used preliminary in the NEIC catalogue, the body wave magnitude m_{pv} from KNDC catalogue, which is derived from the vertical component and for their estimation a local calibration curve was used. As well as the energy class K which represents the logarithm of the seismic energy at the distance of 10 km from epicentre and is mostly used for the classification of the earthquake strength in Russian catalogues. For homogenisation of the catalogue it is necessary to convert different magnitudes to one reference magnitude, which will be used as a standard for the seismic hazard assessment. Of course there are empirical relations from former studies of the region, but it is always advisable to convert the magnitudes from the used dataset, if possible.
These three different magnitudes were converted by linear regression within the database by using the equation

$$M_1 = b + aM_2 + \sigma P \quad (1)$$

where a and b are parameters to be obtained in the regression, M_1 and M_2 are the two scales of magnitude to correlate, σ is the standard deviation and P is zero for 50-percentile values and one for 84-percentile (AMBRASEYS 1990, LOPEZ CASADO et al. 2000).
The dataset contains several magnitudes for events in some time slices. Some periods with different magnitudes are overlap so that for the same event two or even all three magnitudes are available. Such events were filtered from the catalogue. This dataset with filtered magnitudes was split into training and test datasets. Within the training data the conversion of the magnitudes by linear regression was arranged (Fig. 3). Thereafter the

estimated conversion parameters were applied for the test dataset. Due to the fact that for the test data magnitudes from primary estimation were available it is possible to prove the quality of the conversion by testing the residuals between estimated and calculated magnitudes.

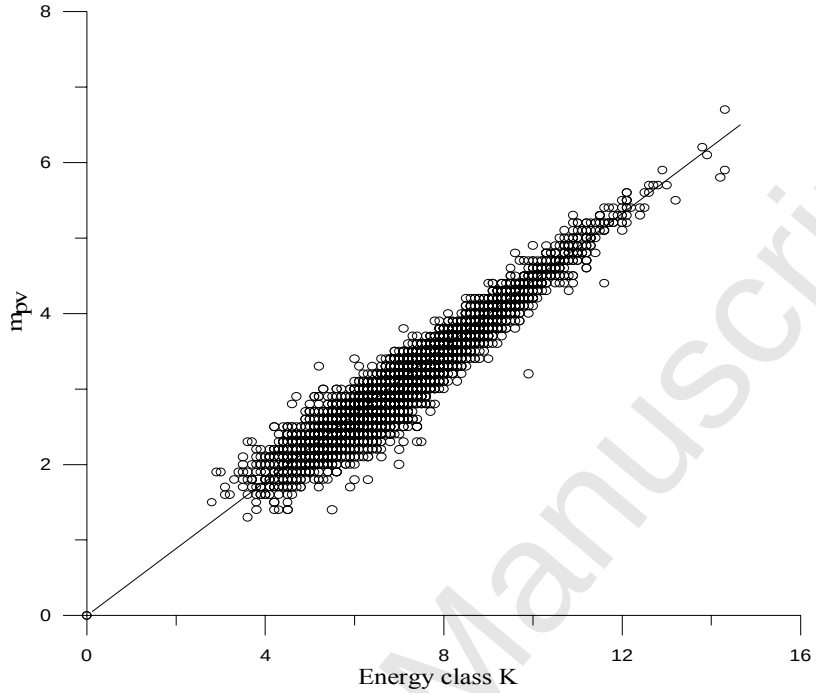

Fig. 2. Conversion of the magnitudes (energy class K to m_{pv}) by linear regression.

The conversion is of different quality. The conversion of m_{pv} to energy class K can be well done with linear regression. The standard deviation is 0.2 and about 95% of all values are within this error that corresponds to the error of primary magnitude estimation (BUNE et al. 1970). Conversion from m_b to m_{pv} is linear only in a range between magnitudes 2.5 and 5.5. Residuals from calculated magnitudes and observed magnitudes are shown in Fig 3. For bigger and smaller magnitudes big standard deviations are needed to process them with linear regression. The results are summarized in Tab. 1.

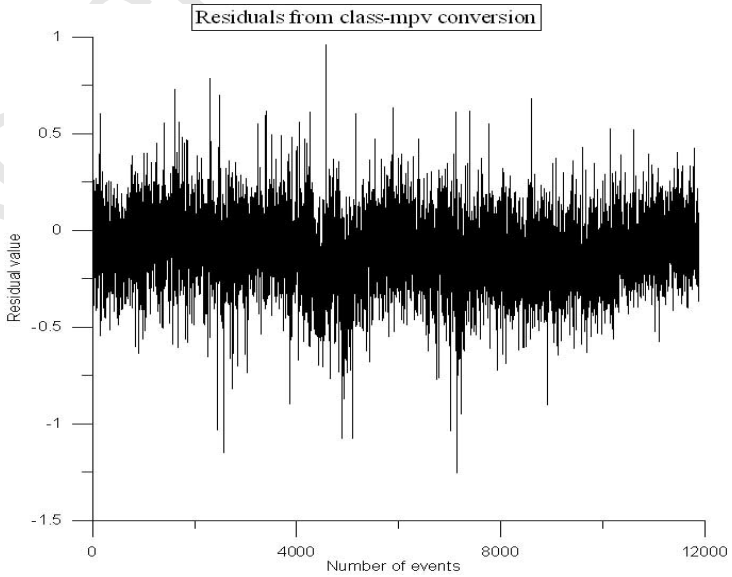

Fig. 3. Residuals from class to m_{pv} conversion.

Tab. 1 Conversion of magnitudes.

Conversion	Regression equation	Standard deviation σ	Values within σ in %
$m_{pv} \Rightarrow m_b$	$m_b = 0.9314*m_{pv} + 0,5$	0.210	84.07
$m_b \Rightarrow m_{pv}$	$m_{pv} = 1.0735* m_b - 0,5$	0.230	84.5
$K \Rightarrow m_{pv}$	$m_{pv} = 0.45*K$	0.204	96.48

5. Seismic density maps

In the first step of the seismic source identification, seismic density maps were created by using kernel density function (DUONG et al. 2008; WASSERMAN 2005; SILVERMAN 1986; EPANECHNIKOV 1969). Kernel density provides different density estimators. The general form of a kernel estimator is:

$$\tilde{f}_{\lambda}(y) = \frac{1}{n\lambda}\sum_{i=1}^{n} K_0\left(\frac{y - y_i}{\lambda}\right) \tag{2}$$

where K_0 is a kernel function and λ is the bandwidth. For this analysis we used the quadratic kernel function:

$$K_0(t) = \begin{cases} \frac{3}{4}(1-t^2) & for|t| \geq 1 \\ 0 \end{cases} \tag{3}$$

Although the kernel density estimation provides different kernel estimators, the choice of the estimator is irrelevant for the statistical performance of the method (EPANECHNIKOV 1969). With a specific kernel function, the value of λ determines the degree of averaging in the estimate of the density function and is called a smoothing parameter.

For the analysis commercial software GIS ArcInfo 9.2 was applied, where the quadratic kernel function is implemented in the toolbox. All seismic events were assumed as point sources in the first approximation. The optimal bandwidth was calculated automatically with the least squares method from the dataset. In simple terms the analysis process can be describe as follows: A smoothly curved surface is fitted over each point. The surface value is highest at the location of the point and diminishes with increasing distance from the point, reaching zero at the search radius distance from the point. Only a circular neighbourhood is possible.

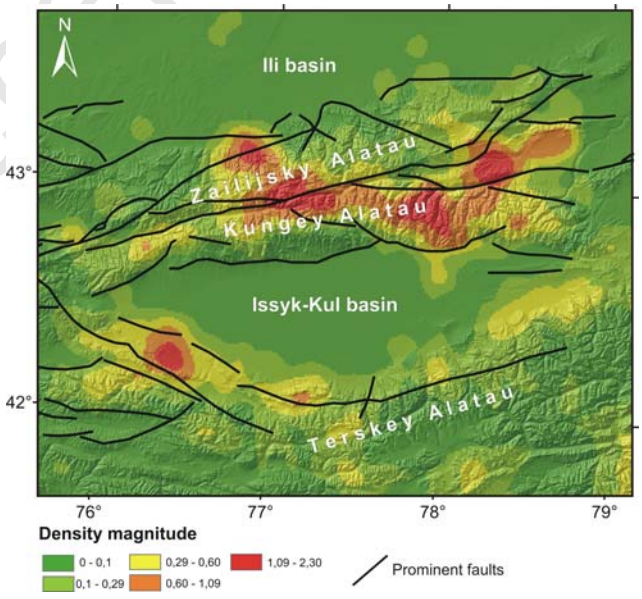

Fig. 4. A 3-D-view of the seismic density map overlain by mapped active faults after DELVAUX et al. 2001.

The density at each output raster cell is calculated by adding the values of all the kernel surfaces where they overlay the raster cell centre. Increasing the search radius will not greatly change the calculated density values. Although more points will fall inside the larger neighbourhood, this number will be divided by a larger area when calculating density. The main effect of a larger radius is that density is calculated considering a larger number of points, which can be further away from the raster cell. This results in a more generalized output raster. The idea of this analysis is that near to the active faults the number of seismic events per area should be higher then in their surroundings. After the calculation of the seismic density the faults known from geologic mapping were overlaid with the density maps (Fig.4).
To analyse the temporal development of the seismicity, seismic density maps were created for the time span 1980 until 2006. This period was chosen because the instrumental observation shows about equal quality and number of events. These annual maps are very helpful to understand the continuity of the activity from earthquake sources and their origin. So, the smooth density gradients with slowly changing shapes through the years point to zones caused by continuously ongoing tectonic processes (active faults). Sudden swarms, like in Fig. 5-1987 can be interpreted as fluid induced earthquakes.

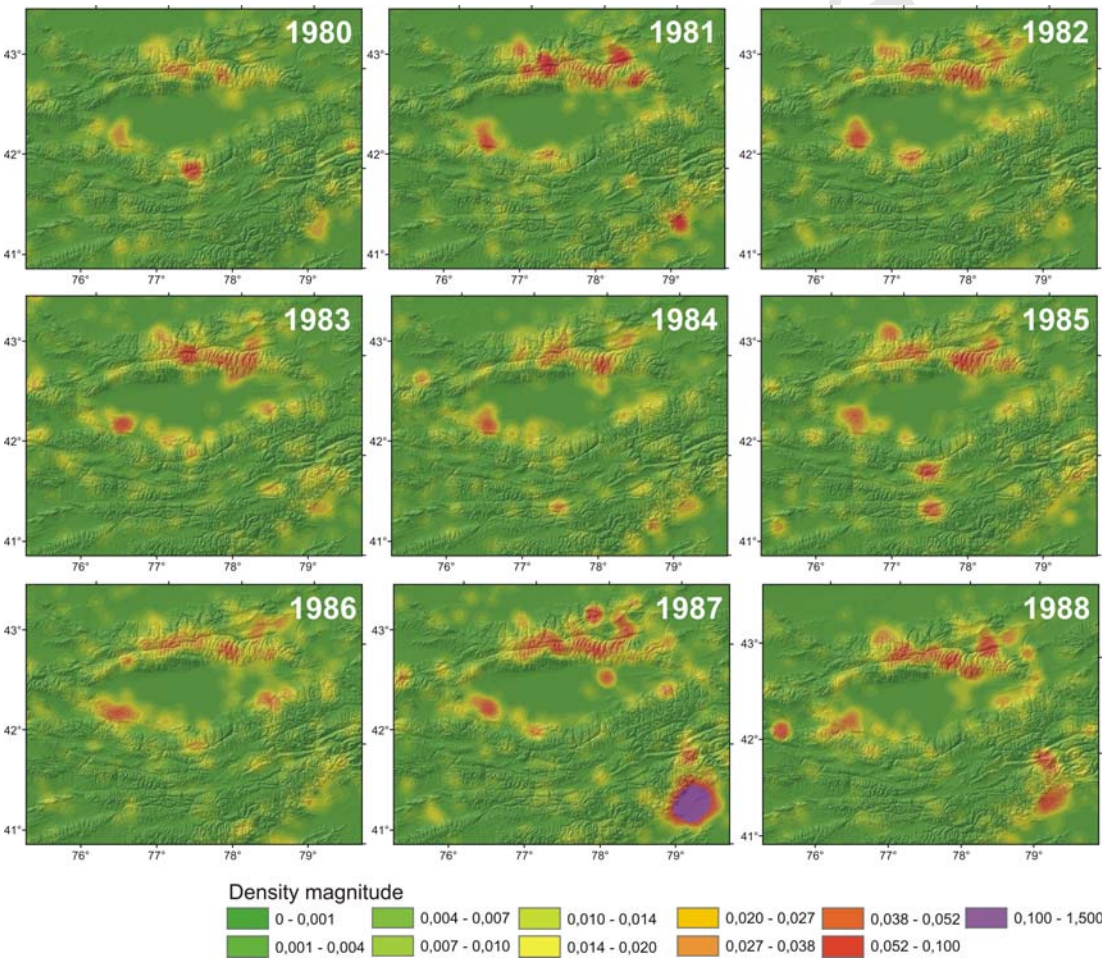

Fig. 5. Sequence of annual seismic density maps of four years from 1980 until 1988: well pronounced is the density shape of the active region in the northern region that corresponds to the ridges Zailijsky and Kungey Alatau. The Issyk-Kul basin shows less seismic activity and is surrounded by a seismic "belt". Shape of this activity zones around Issyk-Kul and northern ridges change only slightly from year to year. On the figure 1987 a circular structure with very high density and high gradient represents a sudden earthquake swarm on the transition zone to the Tarim.

6. Construction of the subsurface fault geometry from GPS data (kinematic approach)

For modern seismic risk studies it is also important to know the fault geometries. Information on fault dips and fault areas improve the accuracy of the seismic source characterisation and the estimation of the seismic hazard

potential of the source within the seismotectonic model. Unfortunately, there are no suitable geologic profiles across the research area. Although there are a plenty of geologic field studies and observations (e.g. MAKAROV et al. 2005; MOLNAR 2000; REIGBER 2001; DELVAUX 2001; ABDRAKHMATOV 1996, 2001) there is no general model, which describes the faults, their activity and their interaction. Even character and dip direction of the faults differ between different authors. This was the reason for using GPS data for fault geometry construction. For other methods of subsurface fault prediction (e.g. GEISER 1988) there are no quantitative observations in the region.

GPS measurements in Tien Shan are carried out since 1992 (MOLNAR 1993; MAKAROV et al. 2005). Today, there are nine permanent stations in Central Asia, three of them are situated in the northern Tien Shan and will be used to fit the data of temporal campaigns which were periodically repeated during the last 15 years. In 2002 the amount of measurement points in whole the Tien Shan area rose to 420 (MAKAROV et al. 2005) and today there are nearly 450 measurement points (BOGOMOLOV et al. 2007). Actually the horizontal displacement map of Central Asia can be downloaded from the UNAVCO (2008) website, a non-profit membership governed consortium. GPS data are actually used by other research groups to correlate strain derived from GPS data and seismic activity of the region (e.g. BOGOMOLOV et al. 2007).

The displacements we used for this work are calculated relative to "stable Eurasia". Figure 6 shows the horizontal velocity field of the Tien Shan. The velocity gradient from south to north is in a range of 10 to 1 mm/year.

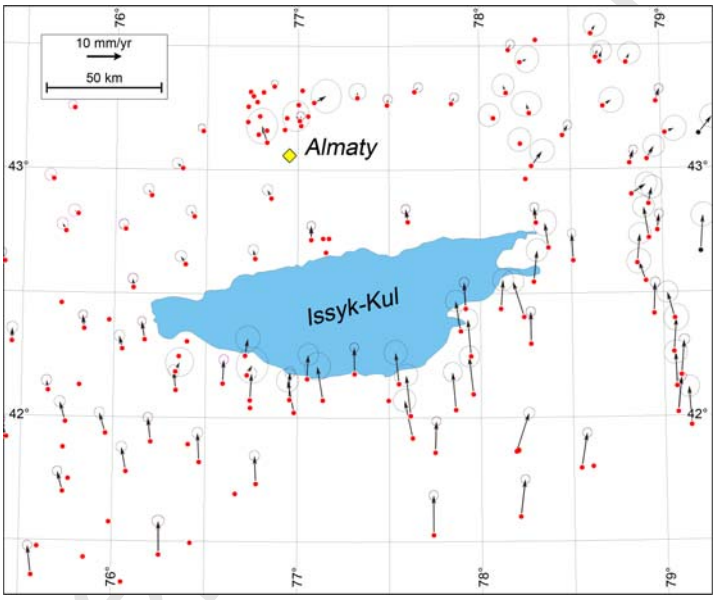

Fig. 6. Horizontal velocity map of the Tien Shan. Circles around the top of the arrows mark the 95% confidence interval (UNAVCO 2008).

The reconstruction method is based on the existing tectonic models of fault parallel flow (e.g. SANDERSON 1982; SAVAGE & COOKE 2003) and was already carried out by TORIZIN (2007) in Diploma Thesis as a possibility to estimate the recent uplift on the northern range of Zailijsky Alatau.

The reconstruction method is based on several fundamental assumptions. First, we assume that all deformation occurs only on the faults and without internal shortening of thrust sheets. For long term we assume that the elastic component in the deformation is absent. The volume in 3-D and area in 2-D during the deformation is constant. It is allowed to shear the rock body parallel to the fault. With these assumptions it is guaranteed that each point displace along the generated "flow lines" that parallel the fault surface within each dip domain. Dip domains are bounded by the angle bisectors to the fault kinks (Fig 8, 9).

We describe the total displacement D in simple terms as a sum of displacement along the fault d, elastic deformation of the material ε and internal shortening of the geological unit F:

$$D = \sum_{i=1}^{n} d_i + \varepsilon + F \tag{4}$$

With the assumption that there is no folding the last term becomes zero. Further we assume that an elastic deformation of material is negligible in proportion to the displacement along the fault. With this assumption equation (4) is simplified to:

$$D = \sum_{i=1}^{n} d_i \tag{5}$$

and for the 3-D case to:

$$|D| = \sum \sqrt{d_i^2 + d_j^2 + d_k^2} \tag{6}$$

With this kinematic perception the velocity gradient measured by GPS can be explained by conversion of the horizontal component into the vertical along the fault surface due to a change of the fault ramp angle (Fig. 8). Fault segments where the fault is sub-horizontal are indicated by equal GPS derived horizontal displacements over broad areas. In this case we can construct the fault geometry at depth from the point where the fault intersects the surface.

The first step of a subsurface fault geometry construction is creating a displacement map. Therefore the displacement vector map from UNAVCO (2008) was recalculated for vector direction relative to N-S orientation and interpolated to a smooth contour map with a contour interval of 1 mm/yr. The created contour map shows only the annual velocity of the north component. Furthermore the complex fault outcrops after DELVAUX et al. (2001) were simplified to general fault zones (Fig. 7). Therefore we generalized all small fault to "fault zones" represented in the model by one discrete fault surface.

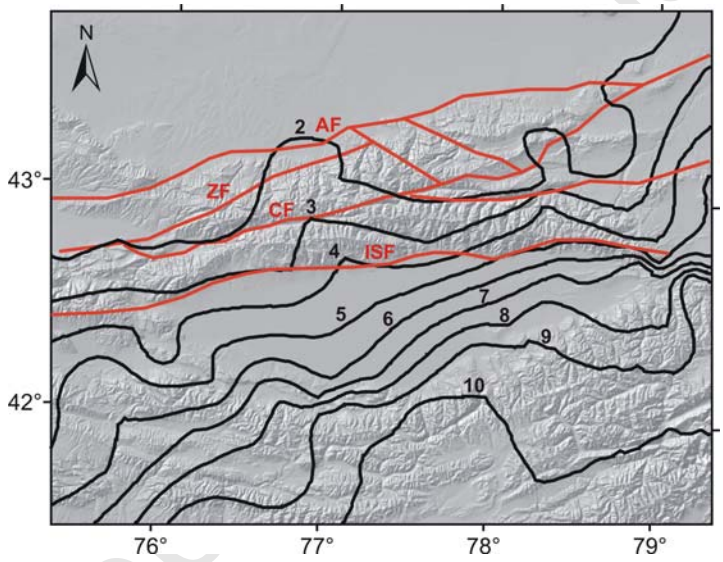

Fig. 7. Contour map of horizontal displacements from GPS data (black lines) and modified active faults after DELVAUX et al. 2001. AF – Almaty Fault, ZF – Zailijskij Fault, CF – Chilik Fault, ISF – Issyk-Kul Fault.

The construction starts by calculating the ramp angles. First it is necessary to locate the flat segment of the fault surface. Low gradients in the displacement contour map indicate this part. The displacement value above this part is taken as a total displacement along the fault surface. With equations 5 to 10 we calculate the angles of the fault ramp α and β and angle between bisector and surface ε'.

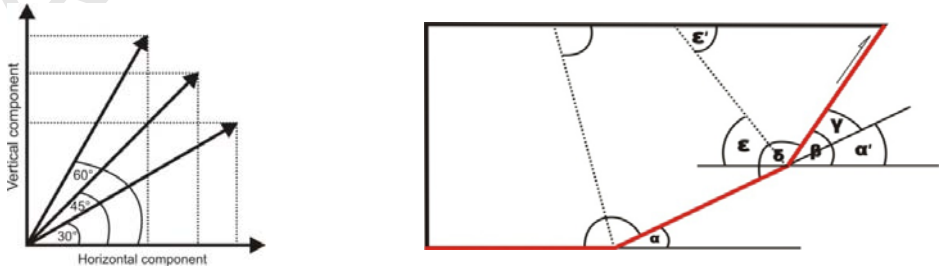

Fig. 8. Principal sketch of the fault geometry construction. On the left hand is the principal consideration of the changing of the horizontal component with rising dip angle. On the right hand the principal sketch of the angle relation to estimate the angles of bisectors to the surface is given. α and β are ramp angles, δ is the included angle of the fault ramp parts, ε' is the angle between the surface and the bisector.

The ramp angles α and β can be calculated from the total displacement D and horizontal displacement d_i within each dip domain or vertical displacement d_k

$$\sin \alpha, \beta = \frac{\sqrt{(D)^2 - (d_i)^2}}{D} = \frac{d_k}{D} \tag{7}$$

For other angles there are the following relations:

$$\alpha' = \alpha\,; \quad \gamma = \beta - \alpha'\,; \quad \delta = 180 - \gamma\,; \; \varepsilon = 180 - (\beta + \frac{\delta}{2})\,; \; \varepsilon' = \varepsilon\,; \tag{8) - (12)}$$

Whereas ε' is the angle for the constraint bisector from the surface to the kink of the fault surface. The ramp angle of the last ramp part is at the same time the dipping angle of the fault at the point where the fault cuts the surface. The contours in the map are the boundaries from the dip domains and therefore an angle bisection of the kinks on the fault profile in the depth.
Starting at the fault outcrop on the surface the subsurface fault geometry can be constructed.

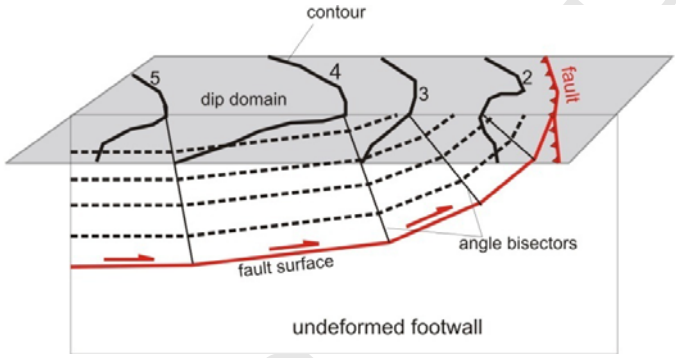

Fig. 9. The principal sketch of the construction of the subsurface fault geometry from the created contour map. Contours show the areas of equal horizontal displacement in mm/a. These are at the same time outcrops of the angle bisectors on the earth's surface. Displacements at every point in the dip domain occur along the "flow lines" (dashed lines) parallel to the fault surface.

The constructed fault has an angular shape that we explain with the resolution of the GPS measurements of 1 mm/year. If it were possible to calculate the gradient with higher accuracy, which means the creation of small scaled contour plots with contour step of less than 1 mm (in ideal infinitesimal) , we would get a change of the fault ramp angle in every point, so that the ramp geometry would become smoothly curving. This corresponds with the fault construction method after ERSLEV (1986, 1991) where the fault ramps were assumed as a circle with the rotational centre above the earth's surface (Fig. 10)

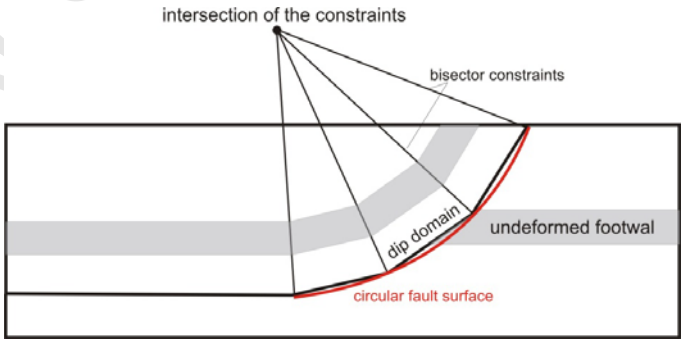

Fig. 10. In ideal the bisector constraints of each dip domain intersect in a common point above the surface. So the angular shaped fault surface can be smoothed by circular shape. The radius of the circle is then given by intersection of the bisector constraints.

7. Results and discussion

A homogeneous composite catalogue of the investigation area was created. Density maps which were calculated using this catalogue provide areas of higher seismicity. The highest seismicity occurs on the Zailijsky Fault and propagates to the north to the Almaty Fault, to the area around Almaty. So we realise that this region is the most active in comparison to the surroundings. But the high seismicity carries no information about the strength of the events. This density map shows only the spatial and temporal distribution of the seismic events along the active faults and can be used to appreciate the activity of certain fault segments. Areas with high seismicity in this map differ in free seismic energy due to the strength of the events which occur there. Moreover, although the complete seismic catalogue was used for the density analysis, it presents only the actual stage of seismic activity, due to the predominant amount of the recorded events after 1980. If we compare the zones of high seismicity with ancient earthquakes, we see that they are partially beside these areas, but not far away (Fig.11). Due to the error of the localisation of ancient earthquakes the small distance to the high seismicity areas is negligible. The biggest events near to Almaty like Verny earthquake 1887 and Kemin earthquake 1911 are completely within high seismic activity zones.

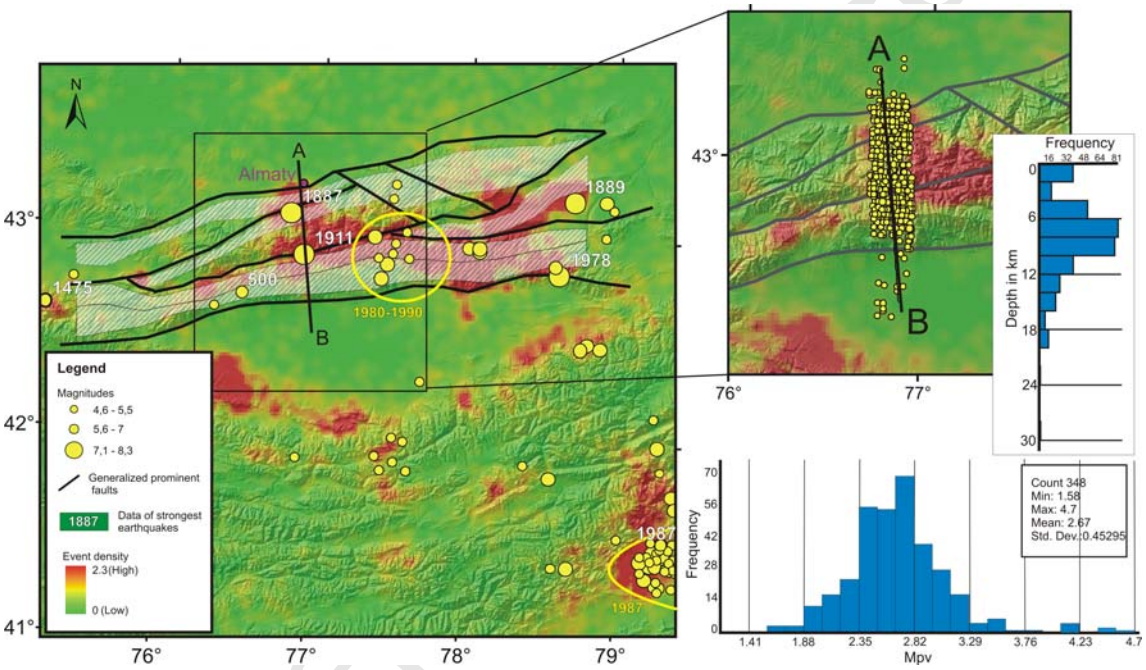

Fig. 11. Left: seismic density map with generalized prominent faults. Shaded areas mark the depth interval 6-18 km at the faults, projected on the surface. Yellow circles mark earthquakes with magnitudes > 4.6. Yellow lines orbit the regions of strong activity in short time periods. Right: aperture of the cross-section A-B with seismic events 5 km around it. Statistics of the depth and magnitude m_{pv} distribution are presented.

But in this context it should not be forget that for the calculation of these zones the events were assumed as point sources, which is not real. As it is well known, rupture zones of bigger earthquakes may reach several hundred kilometres (ULOMOV 1974, CHEN & SCAWTHORN 2002).

A cross-section along the A-B profile shows that the spatial function of seismic density distribution has its peaks above the faults. Thrust faults like Almaty and Zailijsky Fault can be well identified. On the other hand, the back thrusting on the margin of Issyk-Kul basin shows no seismic activity (Fig. 12).

Annual maps for the period from 1980 until 2006 confirm the approach of tectonic origin of the most earthquakes. But they also show sudden earthquake swarms which occur only for short periods and disappear for years. Similar seismic phenomena are known from several areas worldwide (JENTZSCH et al. 2003, KURZ et al. 2003, NAUJOKS et al. 2007) and there is a broad discussion of fluid induced events. KOPNICHEV & SOKOLOVA (2004; 2006; 2007) discuss the importance of fluids in preparation of strong earthquakes in Central Asia, especially in the area near Bishkek (app. 150 km west of Almaty).

In general it can be supposed that most events, also events with magnitudes < 3, are coupled to the fraction processes around active faults. In the comparison of the amount of the events and their distribution there is no significant “background” seismicity beyond active tectonics. In case of this region “background seismicity” is reasonable to use only for engineering importance of the event. The effect of fluid triggered earthquakes cannot

be discussed at the time, because it is still under consideration and fluid triggered processes cannot be yet taken into account in the present seimotectonic model.

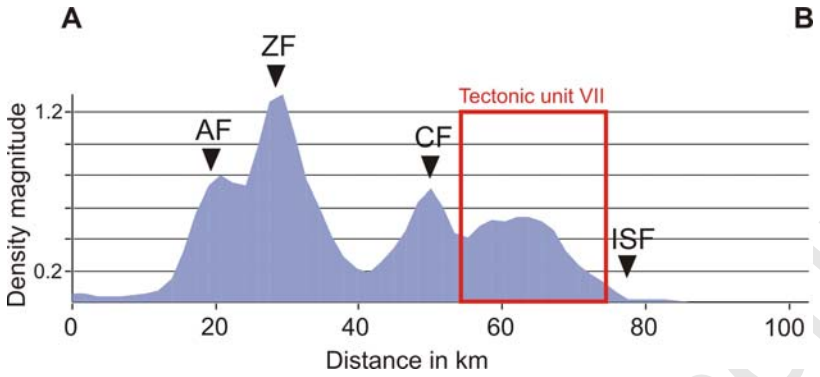

Fig. 12. Cross-section of the seismic density from A to B. The Density function show peaks which correlate with the location of prominent faults. AF – Almaty Fault, ZF – Zailijsky Fault, CF – Chilik Fault. The seismic activity is low and partially absent along the ISF (Issyk-Kul Fault), but the whole tectonic unit VII, which is bounded by CF and ISF, is represented by high and moderate seismic activity.

Comparison of the horizontal velocity contour map with the seismic density map shows an unexpected correlation in the region of Zailijsky Alatau (Fig. 13). The interpolated isoline of the annual velocity of 2 mm bounds exactly the density shape of the seismic map and acts as envelop of the possible deformation front.

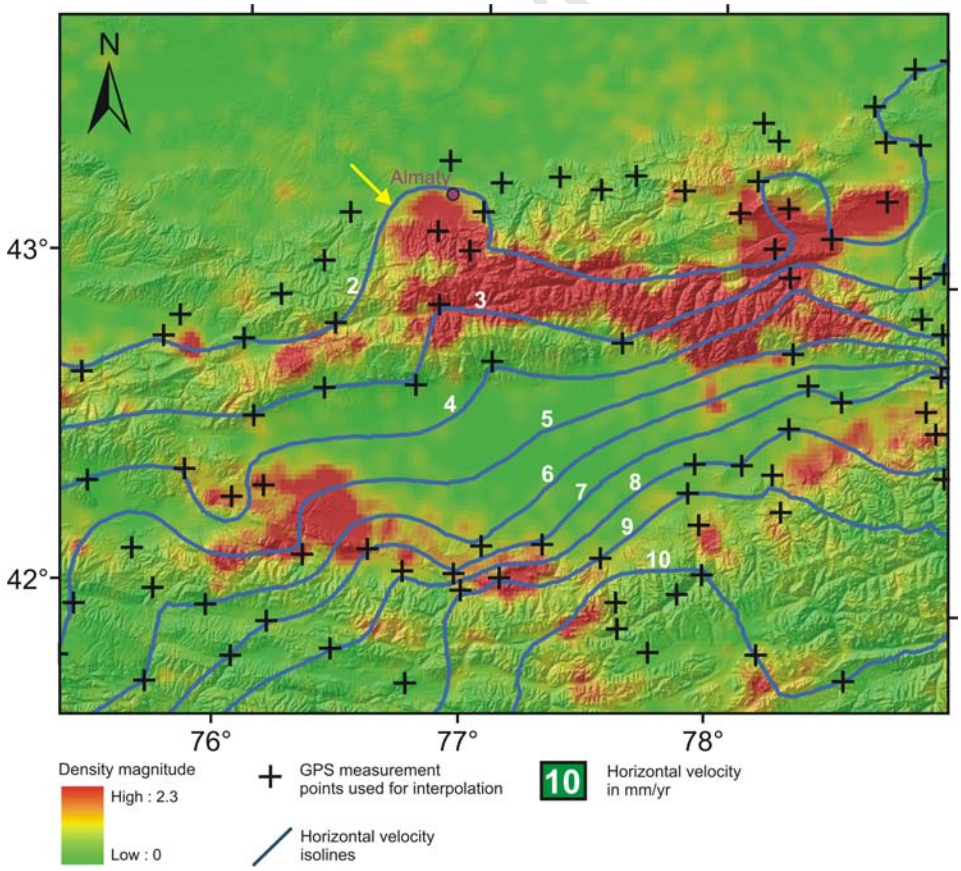

Fig. 13. Seismic density map overlain by contour map of horizontal velocity. Horizontal velocity isolines show correlation in the northern part and built a kind of envelope for the front area of seismic activity (yellow arrow).

The construction of the fault geometry shows steep south dipping faults which have its detachment in depths between 30 and 40 kilometres. The uncertainty made by estimation of the fault geometry given by the vector

displacement field resolution, localisation of the fault outcrop, construction uncertainties and neglecting of viscous processes beneath 15 km depth, can be appreciated in the order of ±10 km. Thus, we assume that the estimation of the flat ramp depth can vary in the range of 10-15 km for deep fault segments. Steep dipping thrust faults with circular fault surface point to reactivation of ancient listric normal faults. This aspect is also discussed by BUSLOV et al. 2004, MAKAROV et al. 2005 and other authors. We constructed only the faults to the north of the Issyk-Kul basin. The Issyk-Kul Fault cannot be constructed with this method and its geometry is only supposed. The best constructed fault is the Chilik Fault for whose construction five bisector constraints are available.

The overlaid seismic tomography from MAKAROV et al. (2005) shows a correlation between the foci of big earthquakes and constructed faults (Fig. 14).

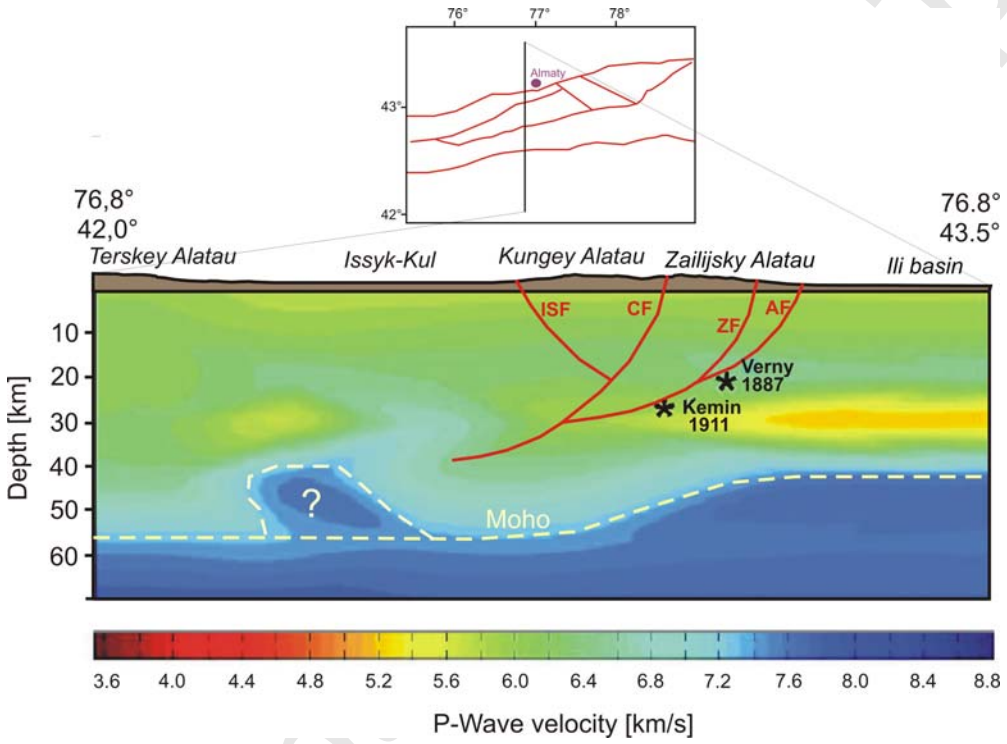

Fig. 14. Seismic p-wave tomography (MAKAROV et al. 2005) overlain by constructed fault geometry and two hypocenters of strong earthquakes marked with stars. Prominent faults are ISF - Issyk-Kul Fault, CF – Chilik Fault, ZF – Zailijsky Fault, AF – Almaty Fault..

The geometry of the faults can explain the spatial distribution of the seismic activity. Peaks of seismic activity overlay the fault in quite short intervals. This may be caused by the material properties which change with increasing temperature and pressure due to increasing depth. Quartz bearing rocks show already ductile behaviour in depths of 15-20 km at the temperature of 600°C (STÜWE 2007) with the consequence of deformation with fewer fractions, lower accumulation and lower seismicity. So the regions where the fault ramp is deeper than 15 km are seismically less active. The average depth of the most events is 8 to15 km, increasing to the south. Increasing of the seismic depth may be caused by different thermal gradients due to the increased crustal thickness beneath the higher mountain chain (VINNIK et al. 2004, 2006; MAKAROV et al. 2005). Low seismicity beneath the Issyk-Kul basin indicates aseismic creep in the ductile upper crust. Here, the construction leads to a fault ramp depth of 30 to 40 km.

The fault geometry and the spatial pattern of the seismic density distribution lead us to suggest a new seismotectonic model of the region of the northern Tien Shan (Fig. 15). This model consists of eight tectonic units which are bounded by big thrust faults. These faults are the main seismic sources in the region. The seismic strength of the event is controlled by the seismic potential of the tectonic units and depth of the fault surface where the rupture occurs. But the density maps show also that not all fault segments are equally active. There are aseismic parts like the Talgar block (compare with Fig. 11) which can have a potential to introduce a strong earthquake in the future. KOPNICHEV et al. (2004) describe aseismic regions of nearly elliptical shape as preparation zones of bigger earthquakes.

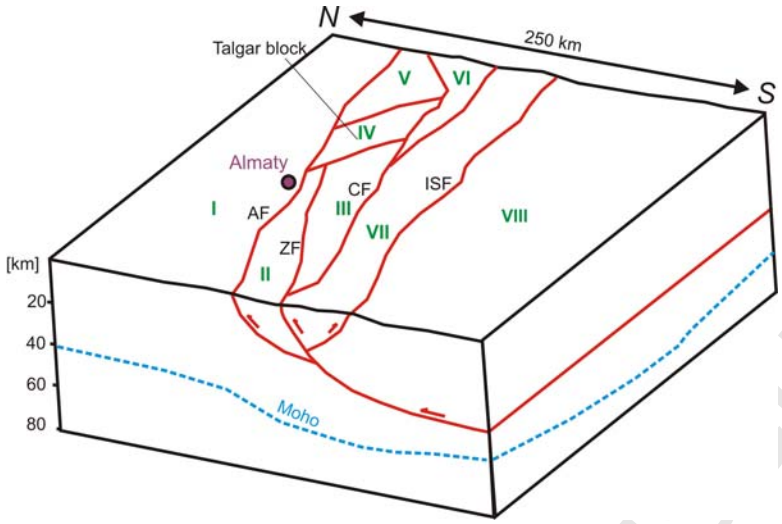

Fig. 15. Seismotectonic model of the region with subsurface fault geometry constructed from GPS-data. Smoothed Moho surface is derived from receiver function tomography (VINNIK et al. 2006). Roman numerals mark tectonic units, which are bounded by faults.

The area to the east of Almaty shows no significant activity in the last time. There are several possibilities to explain this. First, the area has only a small seismic potential due to the cliffy rocks near the surface and lots of smaller faults which penetrate this block deep enough to disturb the stress accumulation. But in this case a lot of small events should be observed here. The completely absence of seismicity in the region which is surrounded by highly active regions is more suitable to interpret as a rigid block which shows only small deformation, and accumulates the stress.

8. Conclusion and recommendations

Geodynamics in Tien Shan is a very complex topic, which cannot be handled in all details within one paper. In the international project "Seismic Hazard Assessment Almaty" we try to understand the processes leading to strong earthquakes from the view of modern geosciences. The preparations for the seismic hazard assessment as well as the possibility to construct fault geometries are only proposals, which will be discussed and improved in the future.

1. The composite historical catalogue was compiled from different catalogues. This catalogue was homogenized.
2. Seismic density maps which allow to rate the seismicity were calculated.
3. Subsurface geometry of the prominent fault zones was constructed for better estimation of the seismic sources.
4. A 3-D Seismotectonic model consisting from different tectonic units was created.

With a described approach we try to create a new geodynamic model of the region, which may improve the seismic hazard assessment for Almaty. The presented seismotectonic model is going be analyzed numerically. Modelled strain will be compared with observations in Kazakh observatories. Created seismic density map, horizontal velocity contour map and additionally data from Kazakh observatories will provide constraints to ensure a realistic modelling.

REFERENCES

1. **ABDRAKHMATOV, K., ALDAZHANOV, S., HAGER, B., HAMBURGER, M., HERRING, T. A. (1996)**: Relatively recent construction of the Tien Shan inferred from GPS measurements of present-day crustal deformation rates, Nature, Vol. 384, Pages 450–453.
2. **ABDRAKHMATOV, K., WELDON, R., THOMPSON, S., BURBANK, D., RUBIN, C., MILLER, M. and MOLNAR, P. (2001):** Origin, direction, and rate of modern compression in the central Tien Shan, Kyrgyzstan. Geologiya I Geofisika (Russian Geology & Geophysics), vol. 42, pp. 1585-1609.
3. **AMBRAYSES. N. N. (1990):** Uniform magnitude re-evaluation of European earthquakes associated with strong-motion records, Earthq. Engng Struct. Dyn. **1**, pp. 1–20.
4. **ANDERSON, G. J. (1979):** Estimating the seismicity from geological structure for seismic-risk studies, Bulletin of the Seismological Society of America, Vol. 69, No. 1, pp. 135-158.
5. **ANDERSON, G. J. and LUCO, J. E. (1983):** Consequences of slip-rate constraints on earthquake occurrence relations, Bulletin of the Seismological Society of America, Vol. 73, No. 2, pp. 471-496.
6. **AVOUAC, J.P., TAPPONNIER, P., BAI, M., YOU, H., WANG, G (1993):** Active thrusting and folding along the northern Tien Shan and Late Cenozoic rotation of the Tarim relative to Dzungaria and Kazakhstan**,** J. Geophys. Res., Vol. 98, pp. 6755-6804.
7. **BOGOMOLOV, L., BRAGIN, V., FRIDMAN, A., MAKAROV, V., SOBOLEV, G., POLYACHENKO, E., SCHELOCHKOV, G., ZEIGARNIK, V., ZUBOVICH, A. (2007):** Comparative Analysis of GPS , seismic and electromagnetic data on the central Tien Shan Territory, Tectonophysics, Vol. 431, pp. 143-151.
8. **BUNE, V. I., VVEDENSKAYA, N. A., GORBUNOVA, I.V., KONDORSKAYA, N.V., LANDYREVA, N. S., and I. V. FEDOROVA (1970):** Correlation of M_{LH} and rn_{pv} by data of the network of seismic stations of the USSR, Geophysical Journal RAS v. 19 No. 5.
9. **BUSLOV, M. M., KOKH, D. A., DE GRAVE, J (2008):** Mesozoic-Cenozoic tectonics and geodynamics of Altai, Tien Shan, and Northern Kazakhstan, from apatite fission-track data, Russian Geology and Geophysics, Vol. 49, pp.648-654.
10. **BUSLOV, M., DE GRAVE, J., BATALEVA, E. A. (2004):** Cenozoic tectonic and geodynamic evolution of the Tien Shan mountain belt as response to India-Eurasia convergence, Extended abstracts: 19th Himalaya-Karakoram-Tibet Workshop, Niseko, Japan.
11. **CHEN, W. & SCAWTHORN, C. (2002):** Earthquake Engineering Handbook, New York.
12. **CORNELL, C. A. (1968):** Engineering seismic risk analysis, Bulletin of the Seismological Society of America, Vol. 58, No. 5, pp. 1583-1606.
13. **DELVAUX, D., ABDRAKHMATOV, K. E., LEMZIN, I. N., STROM, A. L. (2001):** Landslides and surface breaks of the 1911 Ms 8.2 Kemin earthquake (Kyrgyzstan). Russian Geology and Geophysics, Vol. 42, No. 10, pp. 1583–1592.
14. **DUONG, T., COWLING, A., KOCH, I., WAND, M. P., (2008**): Feature significance for multivariate kernel density estimation, Computational Statistics & Data Analysis, vol. 52, issue 9, pp. 4225-4242.
15. **EPANECHNIKOV, V. A. (1969):** Non-parametric estimation of a multivariate probability density, Theory of Probability and its Applications 14, pp 153-158.
16. **ERSLEV, E. A., (1986):** Basement balancing of Rocky Mountain foreland uplifts, Geology, Vol. 14, pp. 259–262.
17. **ERSLEV, E.A.**, **(1991):** Trishear fault-propagation folding, Geology, Vol. 19, pp. 617-620.
18. **GEISER , J., GEISER, P. A., KLIGFIELD, R., RATLIFF, R., ROWAN, M. (1988):** New application of computer based section construction: Strain analysis, local balancing and subsurface fault prediction. The Mountain Geologist 25(2), pp. 47-59.
19. **GHOSE, S., HAMBURGER, M (1998):** Three-dimensional velocity structure and earthquake locations beneath the northern Tien Shan of Kyrgistan, central Asia, Journal of geophysical Research, Vol. 103, NO. B2, pp. 2725-2748.
20. **JENTZSCH, G., M. KORN, and A. ŠPIČÁK, 2003** (Eds.): The swarm earthquakes in the area Vogtland / NW-Bohemia: Interaction of tectonic stress and fluid migration in a magmatic environment (Editorial). J. Geodyn., 35 / 1-2, 1 – 3.
21. **KHROMOVSKIKH,V. S. (1977):** Correlation of Parameters of Coseismic Deformations with the Magnitude and Intensity, in New Catalog of Strong Earthquakes in the USSR (Nauka, Moscow) [in Russian].
22. **KONDORSKAYA, N. V., SHEBALIN, N. V. and KHROMETSKAYA, E. A. (1977):** New catalogue of strong earthquakes in the USSR since ancient world, (Nauka, Moscow) [in Russian].
23. **KOPNICHEV, Y., SOKOLOVA, I (2004):** Spatiotemporal Variations of the S-Wave Attenuation Field in Source Zones of Strong Earthquakes in the Tien Shan Region: Evidence from the Records of Underground Nuclear Explosions, Doklady Earth Sciences, Vol. 395A, No. 3, pp. 461-464.
24. **KOPNICHEV, Y., SOKOLOVA, I (2006):** Grouping of Strong Earthquakes in Central Asia: New Possibilities of Medium-Range Forecast of Seismic Events in the Northern Tien Shan Region, Doklady Earth Sciences, Vol. 411, No. 8, pp. 1324-1326.
25. **KOPNICHEV, Y., SOKOLOVA, I (2007):** Heterogeneities in the Field of Short Period Seismic Wave Attenuation in the Lithosphere of Central Tien Shan, Journal of Volcanology and Seismology, Vol. 1., No. 5, pp. 333-348.
26. **KOSTENKO, N. N. (2001):** Morphology levels and information of the morphology in the central part of Zailijsky-Alatau, Vestnik Kasachskogo Nationalnogo Tekhnicheskogo Universiteta imeni Satpajeva, Vol. 5(28), pp. 113-127, [in Russian].
27. **KURZ, J., JAHR, T. UND JENTZSCH, G. (2003):** Geodynamic modelling of the recent stress and strain field in the Vogtland swarm earthquake area using the finite-element method. J. Geodyn., 35 / 1-2, 247 – 258.
28. **LÓPEZ CASADO, C., MOLINA, S., GINER, J. J. and DELGADO, J. (2000):** Magnitude-Intensity Relationships in the Ibero-Magrebhian Region, Natural Hazards, Vol. 22**,** pp. 271–297.
29. **MAKAROV, V., Editor (2005):** Recent geodynamics of intracontinental areas of collision mountain building (Central Asia), Scientific World, Moscow.
30. **MOLNAR, P (1987):** Inversion of profiles of uplift rates for the geometry of dip-slip faults at depth, with examples from the Alps and the Himalaya, Anales Geophysicae, 5B, pp. 663-670.
31. **MOLNAR, P. & GHOSE, S. (2000)**: Seismic Moments of major earthquakes and the rate of shortening across the Tien Shan. Geophysical Research Letters 27(16), pp. 2377-2380
32. **MOLNAR, P. (1993):** GPS survey of the western Tien Shan, Semi-annual report to the NASA.
33. **NAUJOKS, M., JAHR, T., JENTZSCH, G., KURZ, J., HOFFMANN, Y. (2007):** Investigations about earthquake swarm areas and processes in Dynamic Planet – Monitoring and understanding a Dynamic Planet with Geodetic and Oceanographic Tools (C. Rizos & P. Tregoning, eds), IAG Symposia Series, Vol. 130, pp. 528-535.
34. **PAVLIS, N. K., HOLMES, S. A., KENYON, S. C., FACTOR, J. K. (2008):** An Earth Gravitational Model to Degree 2160: EGM 2008, presented at the 2008 General Assembly of the European Geosciences Union, Vienna, Austria.
35. **REIGBER, C. (2001):** New space geodetic constraints on the distribution of deformation in Central Asia, Earth and Planetary Science Letters, Vol. 191, pp. 157–165.
36. **REITER, L (1990):** Earthquake Hazard Analysis: Issues and Insights, Columbia University Press.
37. **SANDERSON, D. J (1982):** Models of strain variations in napes and thrust sheets; a review, Tectonophysics 88/ 3-4, pp. 201-233.

38. **SAVAGE, H., COOKE, M (2003)**: Can flat-ramp-flat fault geometry be inferred from fold shape?: A comparison of kinematic and mechanical folds, Journal of Structural Geology, Vol. 25, pp. 2023–2034.
39. **SILVERMAN, B. W. (1986):** Density Estimation for Statistics and Data Analysis. Chapman and Hall, London.
40. **STÜWE, K. (2007):** Geodynamic oft the Lithosphere. An Introduction, 493 p., 270 illus..
41. **TORIZIN, J. (2007):** Qualitative und quantitative Modelle für rezente Deformation im Nord-Tien Shan auf der Grundlage der Satellitenbilder, digitaler Geländemodelle und geophysikalischer Daten, Institute of Geosciences, University of Jena, Germany.
42. **ULOMOV, V.** I. (1974): Dynamic of the Earth's Crust in Central Asia and Earthquake Forecast, 218 p. Tashkent [in Russian]
43. **ULOMOV, V. I., and the GSHAP Region 7 working group (1999):** Seismic hazard of Northern Eurasia. Annali di Geofisica, vol.42, pp. 1023-1038.
44. **VINNIK, L.P., ALESHIN, I.M., KABAN, M. K., KISELEV, KOSAREV, G. L., ORESHIN, S. I., REIGBER, C (2006):** Crust and Mantle of the Tien Shan from Data of the Receiver Function Tomography, Physics of the Solid Earth, Vol. 42, No. 8, pp. 639-651.
45. **VINNIK, L.P., REIGBER, C., ALESHIN, I. M., KOSAREV, G. L., KABAN, M. K., ORESHIN, S. I., ROECKER, S. W.(2004):** Receiver function tomography of the central Tien Shan, Earth and Planetary Science Letters, Vol. 225, pp. 131– 146.
46. **WASSERMAN, L. (2005):** All of Statistics: A Concise Course in Statistical Inference, Springer Texts in Statistics.

Online seismological bulletin of Kazakh National Data Centre: www.kndc.kz
U.S. Geological Survey catalogues: National Earthquake Information Centre (NEIC): www.usgs.gov
National Oceanic and Athmospheric Administration (NOAA): www.noaa.gov
Global Centroid Moment Tensor Catalogue: www.globalcmt.org
International Centre of Global Earth Models: http://icgem.gfz-potsdam.de/ICGEM/ICGEM.html
UNAVCO: www.unavco.org